Front. Earth Sci. 2015, 9(2): 202–208
DOI 10.1007/s11707-014-0478-z

RESEARCH ARTICLE

The most typical shape of oceanic mesoscale eddies from global satellite sea level observations

Zifei WANG[1], Qiuyang LI[1], Liang SUN (✉)[1,2], Song LI[1], Yuanjian YANG[1,3], Shanshan LIU[1,2]

1 Key Laboratory of the Atmospheric Composition and Optical Radiation, CAS, School of Earth and Space Sciences, University of Science and Technology of China, Hefei 230026, China
2 State Key Laboratory of Satellite Ocean Environment Dynamics, Second Institute of Oceanography, State Oceanic Administration, HangZhou 310012, China
3 Key Laboratory of Atmospheric Sciences and Satellite Remote Sensing of Anhui Province, Anhui Institute of Meteorological Sciences, Hefei 230031, China

Abstract In this research, we normalized the characteristics of ocean eddies by using satellite observation of the Sea Level Anomaly (SLA) data to determine the most typical shape of ocean eddies. This normalization is based on modified analytic functions with nonlinear optimal fitting. The most typical eddy is the *Taylor* vortex (~50%), which exhibits a Gaussian-shaped $\exp(-r^2)$ SLA and a vorticity distribution of $(1-r^2)\exp(-r^2)$ as a function of the normalized radii r. The larger the amplitude of the eddy, the more likely the eddy is to be Gaussian-shaped. Furthermore, approximately 40% of ocean eddies are combinations of two Gaussian eddies with different parameters, but the composition of these types of eddies is more like a quadratic eddy than a Gaussian one. Only a small portion of oceanic eddies are pure quadratic eddies ($< 10\%$) with the same vorticity distribution as a *Rankine* vortex. We concluded that the *Taylor* vortex is a good approximation of the typical shape of ocean eddies.

Keywords sea level anomaly, ocean eddies, *Taylor* vortex, typical shape

1 Introduction

Recent satellite observations have revealed that the world ocean surfaces are mostly occupied by oceanic mesoscale eddies (Chelton et al., 2007). As a dominant phenomenon in the upper ocean, these mesoscale eddies play important roles in ocean dynamics (Roemmich and Gilson, 2001; Chelton et al., 2011a; Dong et al., 2014) as well as in ocean chlorophyll concentrations (Chelton et al., 2011b). A fundamental problem is developing a method to determine the parameters characteristic of ocean eddies. Knowledge of such parameters is important for not only the description of the ocean eddy shape (Chelton et al., 2011a), but also the determination of the composition of the 3-dimensional structures of eddies (Chaigneau et al., 2011; Dong et al., 2012; Yang et al., 2013; Zhang et al., 2013) because the composition method requires the shape parameters to be in terms of the appropriate length scales. The composition of the 3-dimensional structures of eddies is very useful for both theoretical studies and model simulations (e.g., Early et al., 2011).

To solve the above problem, the shapes of mesoscale eddies in combined eddies were investigated by normalizing the Sea Level Anomaly (SLA) data within each eddy by its amplitude A_0 (negative for cyclones and positive for anticyclones), and then normalizing the spatial coordinates of each eddy by the vorticity-based length scale L of the eddy (Chaigneau et al., 2011; Chelton et al., 2011b; Yang et al., 2013; Zhang et al., 2013). Because both the amplitude A_0 and the length scale L are easily obtained from the eddy identification data, we consider this a "direct normalization method."

Using these approaches, doubly normalized SLA profiles were obtained with normalized amplitudes and normalized radii (r), but the results are too diverse to rely on. The normalized profiles (the mean and the mode) generate a variety of shapes (Chelton et al., 2011a). The mean profile is a Gaussian function $\exp(-r^2)$ for 2 out of 3 of the eddy interiors ($r < 2/3$). In contrast, the mode profile indicates a quadratic structure $1-r^2$ within the eddy ($r < 1$). A recent paper (Zhang et al., 2013) claimed that the mesoscale eddies in the ocean exhibit a universal structure.

Received March 28, 2014; accepted June 2, 2014

E-mail: sunl@ustc.edu.cn; sunl@ustc.edu

Horizontally, the pressure anomaly profile is well described by a function of the normalized radial distance from the eddy center $(1-r^2/2)\exp(-r^2/2)$. How do we reconcile these paradoxical results?

After revisiting the above-described normalization method, we found that the parameters may be inaccurate when using the direct identification method, and that two shift parameters should be added to the normalizations. The first shift parameter is the horizontal shift. In general, the eddy center might not be located exactly at the grid point, which implies that the choice of any point as the eddy center might introduce some errors. As a result, the calculated length scales might exhibit some errors. The second shift parameter is the amplitude shift. The background flow might shift the SLA values (Early et al., 2011), making it difficult to identify the exact amplitude.

The identified method may also affect the result. Chelton et al. (2011a) used an SLA-based identification method in which several closing eddies may be identified as a multinuclear eddy. That is, the identified eddy described by Chelton et al. (2011a) might be a mixture of different eddies. Zhang et al. (2013) used a vorticity-based (Okubo–Weiss parameter) method (Isern-Fontanet et al., 2003; Chaigneau et al., 2008; Chelton et al., 2011a), which may avoid the parameter-shift problem via differentiation, but some other problems remain (Chelton et al., 2011a). For example, the interiors of eddies defined by the closed contours of the Okubo–Weiss parameter do not generally coincide with the closed contours of the SLA (Chaigneau et al., 2008; Chelton et al., 2011a).

The motivation for this study is to understand the paradoxical results in determining the structure of ocean eddies, and to find the main eddy types in the ocean. To this end, we used two new procedures. First, we used a mononuclear eddy identification method (Li et al., 2014) to avoid the problem faced by Chelton et al. (2011a). Moreover, it is difficult to directly determine the parameters due to the various noises in the SLA data and the coarse spatial resolution. Instead, we obtain the parameters by a nonlinear optimal fitting approach. We call this new method the "optimal normalization method."

2 Data and methods

2.1 Data

The SLA data used here was from the merged and gridded satellite product of MSLA (Maps of Sea Level Anomaly), which is produced and distributed by AVISO (http://www.aviso.oceanobs.com/) based on TOPEX/Poseidon, Jason 1, ERS-1, and ERS-2 data (Ducet et al., 2000). Currently, the products are available on a daily-scale with a $0.25° \times 0.25°$ resolution in the global ocean. Those data were corrected for all geophysical errors. In this work, the SLA data used were from July 5th, 2006 to Jan 19th, 2011, corresponding to a total of 1,660 days/maps of observations.

2.2 Method

The ocean eddies were identified by the SLA extremes and a sufficient number of neighboring regions similar to those of the previous method (Chelton et al., 2011a), except that the amplitude of the eddy was required to be larger than 3 cm and subjected to a mononuclear eddy constraint (Li et al., 2014). Compared with the smaller amplitude cut-off values used in previous studies, the present values were as large as the measurement error of the SLA data (Ponte et al., 2007). Thus, fewer eddies may have been identified than in the previous studies. On average, there were approximately 3,200 eddies per map, over 5 million in total (Li et al., 2014).

We sampled the profiles of the eddy shapes from the horizontal section. The horizontal x axis is the horizontal distance from the center, which is chosen at the largest amplitude (SLA maximum or minimum). The north-south profiles were abandoned because there is no anisotropy of the eddy shape in the orthogonal east-west and north-south cross sections (Chelton et al., 2011a). The vertical axis h is the SLA of the corresponding point.

In this study, we used the "optimal normalization method" to normalize the eddies. For the first step, we used the analytical profiles to fit the observed profiles to eliminate the observation errors. As we know, the center of the eddy is not always located exactly at a pixel point, and the background geostrophic flow might shift the SLA height. For each eddy, the shape profile was taken from the observed data pairs of the displaced position x from the eddy extreme and its sea level anomaly height, h.

2.3 Models

The equation for the sea level anomaly height h of the analytical Gaussian type eddy is as follows:

$$h = A\mathrm{e}^{-\frac{(x-x_0)^2}{L_e^2}} + B, \tag{1}$$

where A and L_e are the amplitude and the e-fold length scale of the eddy, respectively. Compared to the previous study, two parameters, x_0 and B, were added as the horizontal (position) and vertical (amplitude) shifts, respectively. The vorticity of the eddy in the geostrophic approximation is

$$\xi = \frac{4gA}{fL_e^2}\left[1-\frac{(x-x_0)^2}{L_e^2}\right]\mathrm{e}^{-(x-x_0)^2/L_e^2}, \tag{2}$$

where g and f are the gravity acceleration and rotation parameters, respectively. The vorticity formula is the *Taylor* vortex in classical fluid dynamics (Wu et al., 2006).

Such a profile is also exactly the universal structure obtained in Zhang et al. (2013). The only difference is that Zhang et al. (2013) used the vorticity-based length scale $L = \sqrt{2}L_e/2$ in their studies, where L is the radius at which the axial speed of an axisymmetric Gaussian eddy is maximal, and hence the relative vorticity is zero (Chelton et al. 2011a). Note that the vertical shift B vanishes in Eq. (2). Similarly, the equation for the analytical quadratic type eddy is as follows:

$$h = A\left[1 - \frac{1}{2}\frac{(x-x_0)^2}{L_e^2}\right] + B. \quad (3)$$

The vorticity of the quadratic type eddy is the *Rankine* vortex in classical fluid dynamics (Wu et al., 2006).

For each profile, we used Eq. (1) or Eq. (3) to fit the data, and we determined the eddy type based on which condition passed the fitting examination. The smaller the residue is, the better the model is. The parameters A, B, x_0, and L_e were obtained from nonlinear fitting. If the eddy failed to fit the data, we classified it as the rest type.

Next, we normalized the eddy shape (for each type of eddy) by the following formula:

$$h_n = \frac{h-B}{A},\ x_n = \frac{x-x_0}{L_e}. \quad (4)$$

Figure 1(a) shows a profile of an eddy and its best fit. There is a notable shift and asymmetry, which may due to the movement of the eddy or other influences. The normalized profiles obtained by the direct method and by the optimal method are depicted in Fig. 1(b). It is obvious that the profile from the optimal method is very close to the ideal Gaussian function.

3 Results

3.1 Gaussian shape

First, there are many eddies of Gaussian type. Figure 2(a) shows a profile of the typical Gaussian-type eddy. It is clear that the eddy shape can be well fitted by a Gaussian function, with $A = 21$ cm, $L_e = 60.4$ km, $B = 1.8$ cm and $x_0 = 1.8$ km. This eddy has a perfect Gaussian function profile, and the position shifts are comparably small.

We normalized the Gaussian eddies using the "optimal normalization method". Each point was normalized using Eq. (4). We drew the points as the probability density function in Fig. 2(b). The points cluster into a perfect Gaussian function where the density of the scatter points has three local maxima at $x_n = 0$ and $x_n = \pm\sqrt{2}/2$.

3.2 Quadratic shape

Second, as found by Chelton et al. (2011a), there were quite a few quadratic eddies, i.e., the Rankine vortex in our study. As shown in Fig. 3(a), the second type of typical eddy is the quadratic type. It is well-known that the nucleus of the eddy acts as a solid rotation fluid.

We normalized the quadratic eddies using the "optimal normalization method". Each point was normalized using Eq. (4). We drew the points as the probability density function, as shown in Fig. 3(b). The points clustered into a perfect quadratic function.

3.3 Rest shape

There are many eddies that cannot be easily classified into

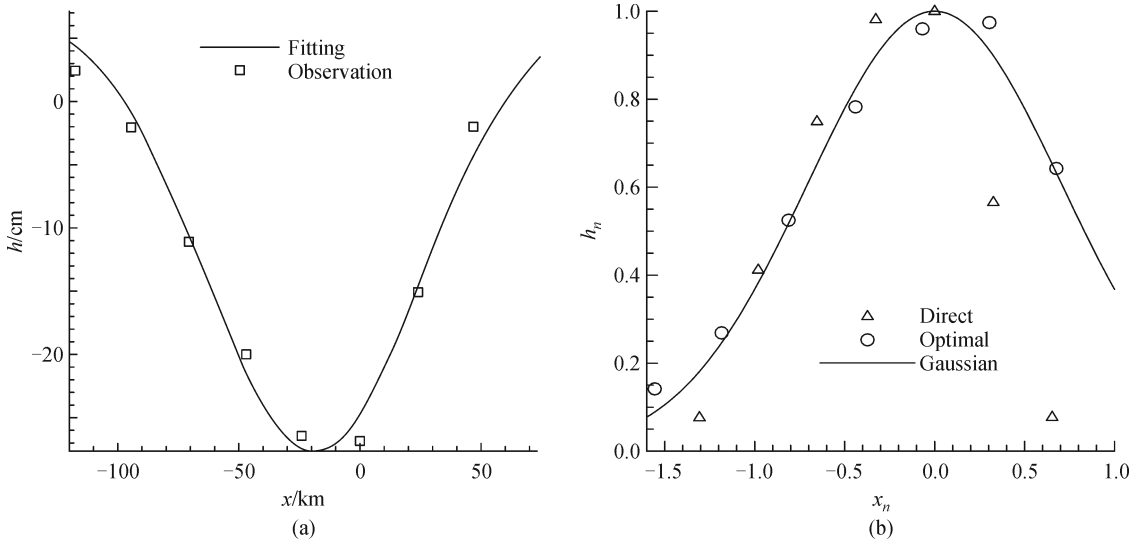

Fig. 1 (a) A typical Gaussian eddy profile (squares) and fitting profile (curve) with $A = -35.1$ cm, $L_e = 62.8$ km, $B = 7.4$ cm and $x_0 = -19.1$ km. (b) The profiles of the direct normalization (triangles) and the optimal normalization (circles) are shown, and the curve is the profile from the normalized Gaussian function.

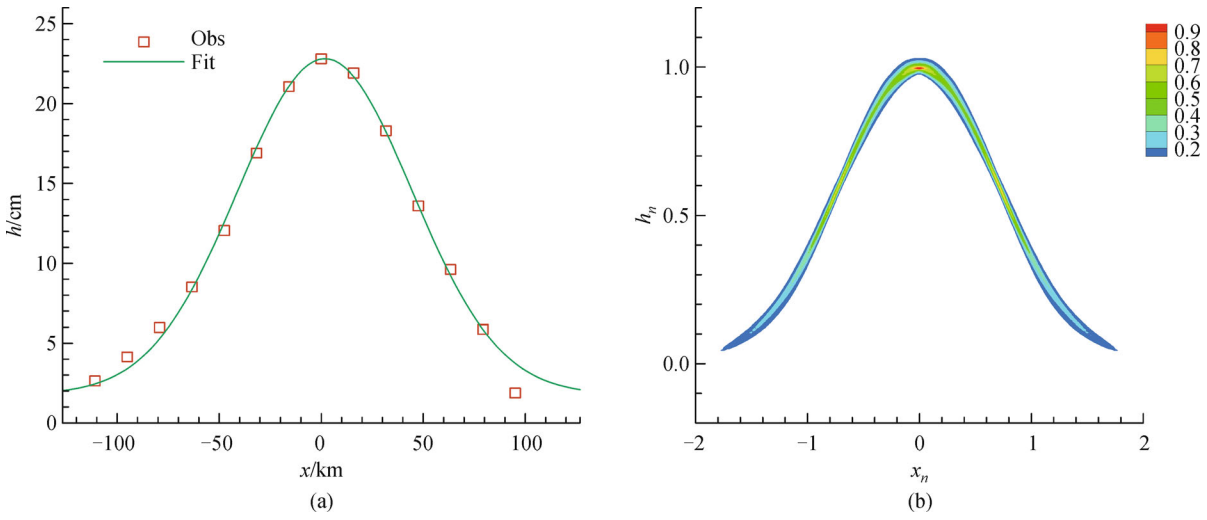

Fig. 2 (a) A typical Gaussian eddy profile with A = 21 cm, L_e = 60.4 km, B = 1.8 cm and x_0= 1.8 km. (b) Probability density function distribution of the normalized SLA shape for Gaussian eddies.

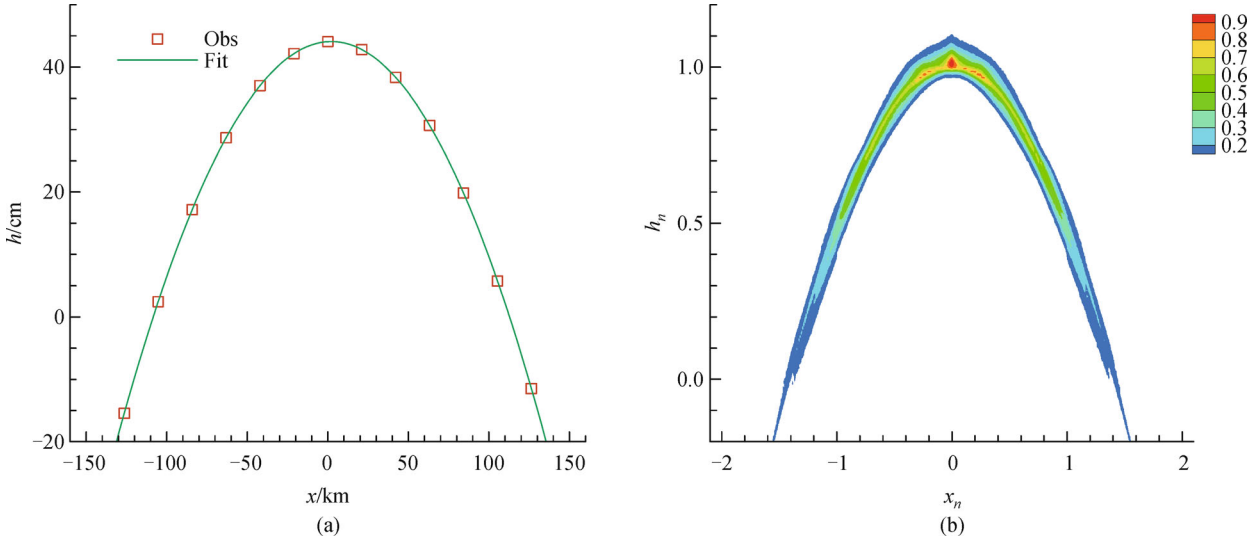

Fig. 3 (a) A typical quadratic eddy with A = 61.8 cm, L_e= 92.6 km, B = −17.7 cm, and x_0= 2.2 km; (b) Probability density function distribution of the normalized SLA shape for quadratic eddies.

either of these two simple types of eddies. We classify such eddies as the rest type. Most of these eddies might be combinations of a simple-type eddies. Figure 4(a) shows a combination of two Gaussian-shaped eddies with different parameters. The combination eddies are very common in the ocean, where two eddies are often too close to be separated.

The composite eddy of the rest type is quite different from the above ones, as is shown in Fig. 4(b). The combination eddies have binary profiles. The center of the binary profiles is more like a quadratic eddy than a Gaussian eddy. This similarity to a quadratic eddy may be the reason why the mode profile obtained was quadratic.

3.4 Shape potions

Finally, we simply classified all eddies into three typical types: the Gaussian eddy, quadratic eddy, and the rest. Next, we calculated the amplitudes of the different eddies. Similar to the previous results, as the amplitude decreased, so did the number of eddies.

As shown in Fig. 5, the Gaussian type eddies comprised more than half of the total analyzed eddies. As the amplitude increased, so did the ratios of the Gaussian eddies to the quadratic eddies and to the rest. When the amplitude was 5−15 cm, only approximately half of the eddies were Gaussian. This percentage increased to near

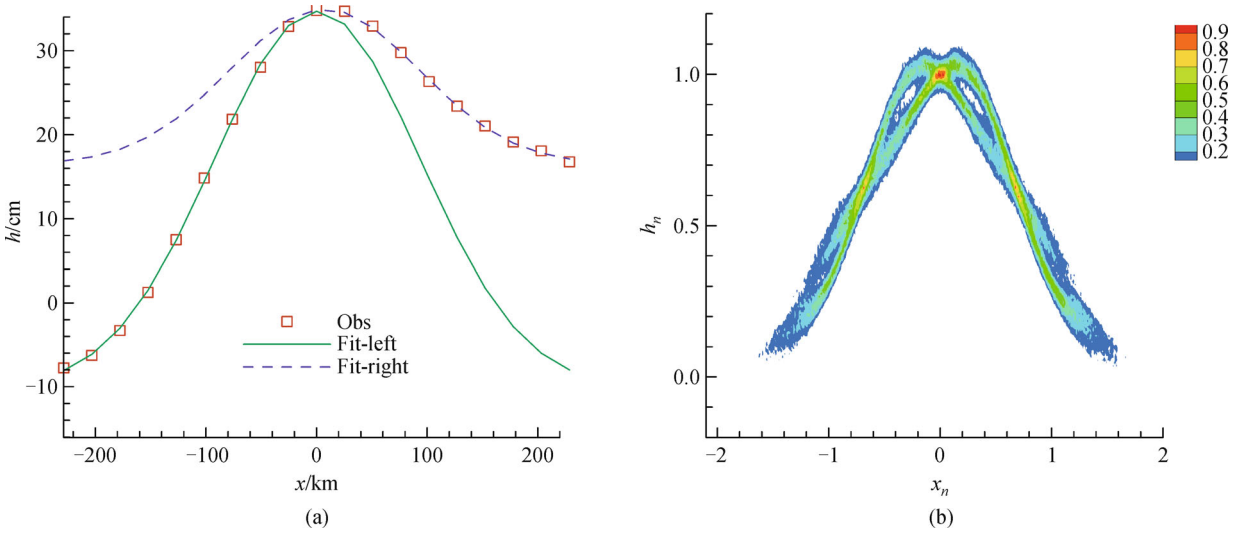

Fig. 4 The rest type of eddies. (a) A combination eddy consisting of two Gaussian eddies (left: $A = 45$ cm, $L_e = 132.2$ km, $B = -10.3$ cm and $x_0 = 0.65$ km; right: $A = 18.5$ cm, $L_e = 121.3$ km, $B = 16.46$ cm and $x_0 = 7.24$ km). (b) Probability density function distribution of the normalized SLA shape of Gaussian eddies.

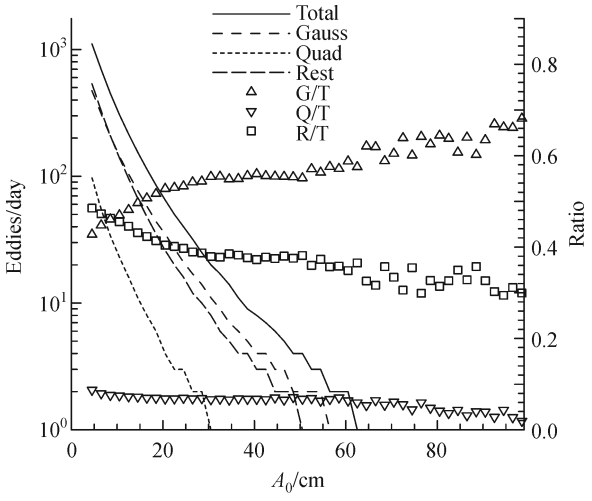

Fig. 5 Numbers of eddies per map and ratios of the different types of eddies.

70% as the amplitude increased to 100 cm.

Furthermore, the quadratic eddies comprised a small portion of the total eddies ($< 10\%$). The rest eddies comprised approximately 40% of the total eddies, and their portion decreased from 60% to 30 as the amplitude increased. Among these rest eddies, most were a combination of two Gaussian eddies with different parameters. Note that the mononuclear eddy method can identify approximately 30% to 40% more eddies than the multinuclear eddy method (Li et al., 2014), which is consistent with the present results.

Overall, most of the ocean eddies are of the simplest type: the Gaussian-shaped *Taylor* vortex. The larger the amplitude is, the greater the ratios of the Gaussian-shaped eddies to the quadratic eddies and to the rest.

4 Discussion

Comparing these results with the previous composition method (Chelton et al., 2011a; Zhang et al., 2013), the results of the present study can explain the controversial results between them. Because shifts exist, the results might be as diverse as those of the direct composition method (Fig. 1). The method used by Zhang et al. (2013) is better than that of Chelton et al. (2011a) because the vertical shift parameter automatically vanishes, which may induce significant errors, as indicated by the following discussion. Most importantly, we used the optimal fitting parameters as the length scales. It was obvious that the identified parameters were easily affected by the observation errors and resolution errors. For example, the directly identified L requires the calculation of the differentiation of the SLA. As noted by Chelton et al. (2011a), the differentiation amplifies the noise in the SLA field. The comparisons of the parameters in Figs. 1−4 clearly show that optimal fitting is required to obtain the proper parameters. The shape of the combination of Gaussian eddies also indicates that their simple composition can result in these eddies being mistakenly classified as quadratic eddies.

In addition, we added two parameters to eliminate the observation shift errors which were ignored by the previous studies. If the ratios of B/A and x_0/L_e were relatively small (e.g., < 0.1), then the graph using Eq. (4) was very similar to that using the previous method. As we

can see from Fig. 1(a), the position shifts were quite large in some cases.

Figure 6 shows the probability density function distribution of the parameters and their shifts. The amplitude shift "B" was primarily less than 6 cm, which is much larger than the observation data error (~ 3 cm). In Fig. 6(b), the mean of shift B was very small (< 1 cm), while the standard deviation, δ, of B was quite large (~10 cm). The ratio δ/A decreased from 1 to 0.1 as the amplitude increased from 10 cm to 100 cm. The horizontal position shift was primarily less than 5 km in Fig. 6(c). The mean of the shift x_0 was very small (< 2 km), while the standard deviation, δ, was relatively large (10−20 km). The ratio δ/A decreased from 0.4 to 0.1 as the length scale increased from 25 km to 200 km.

As mentioned in the Methods Section, the ratios of B/A and x_0/L_e should be relatively small for the previously used method. However, the above results illustrate that they were not as small as we had expected. This discrepancy is why direct normalization would be inaccurate for determining the eddy shape. In conclusion, the shift parameters are required for fitting the eddy shape.

It is interesting that the vorticity of the Gaussian eddy in Eq. (2) has the same distribution (but different length scale) as that of the pressure anomaly found in a recent work (Zhang et al., 2013). In their model, the vertical structure has a nonzero phase at the surface, which was presumed to be due to differential surface dynamics. According to the present work, the SLA could exhibit such shape and could naturally be associated with a similar vorticity distribution. This result implies that the measurements of SLA and density profile might be used to derive the 3-dimensional structure of the eddy in future work (Hu et al., 2011; Dong et al., 2012).

On the one hand, the vertical structure was found to be only one simple sinusoid profile (Zhang et al., 2013). On the other hand, both the field observation (e.g., Hu et al., 2011; Dong et al., 2012) and theoretical work (Sun, 2011)

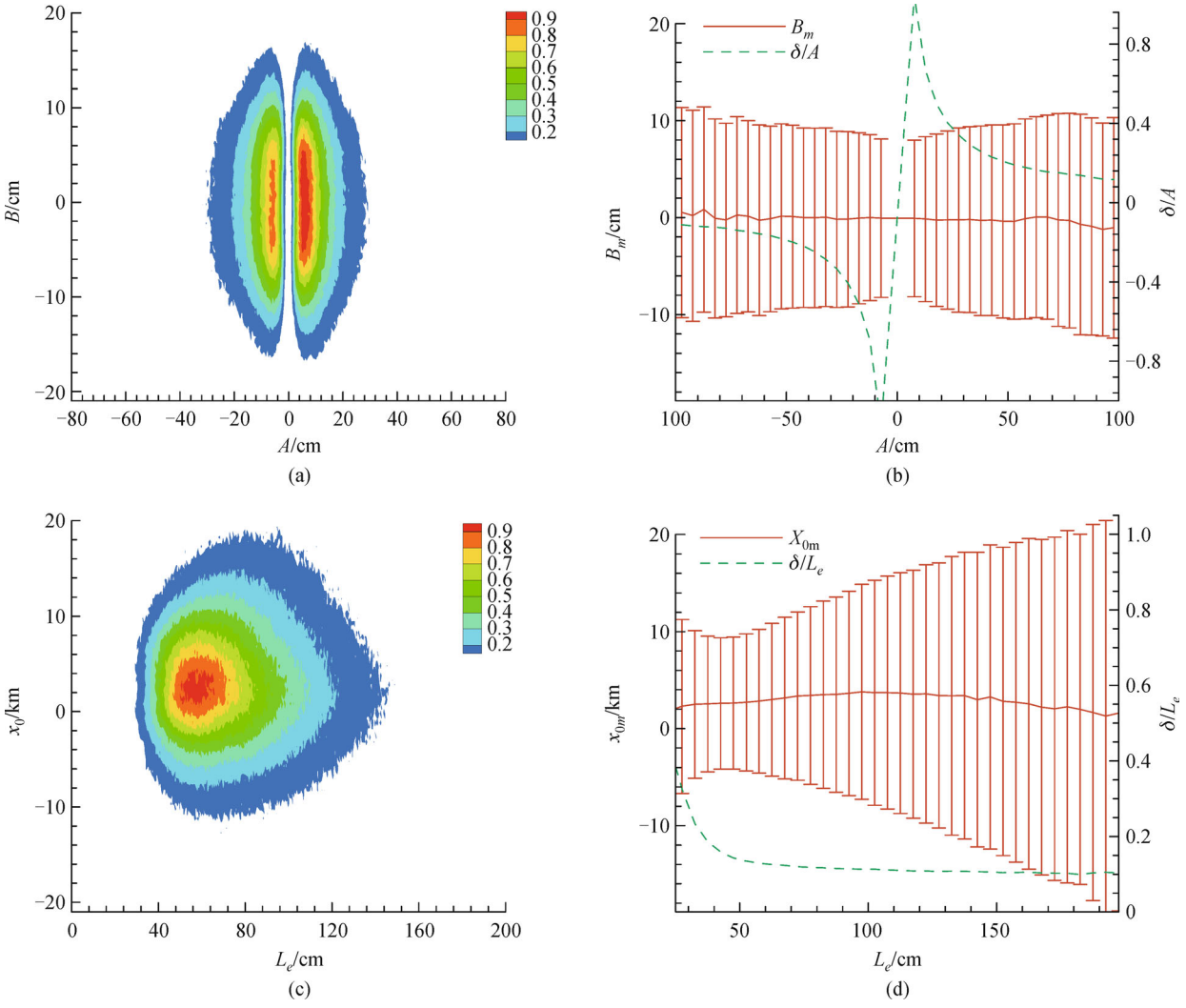

Fig. 6 (a) Distribution of B and A of the eddies. (b) Mean and standard deviation of B vs. A. (c) The distribution of x_0 and L_e of the eddies. (d) Mean and standard deviation of x_0 vs. L_e.

revealed that the vertical structure of the eddy may be described by other laws. Are there other possible vertical profiles in the ocean? This question remains an open problem for further studies. Moreover, the eddy structure could be self-similar in both horizontal and vertical directions. Accordingly, the separation of variables could be used in the theoretical eddy models, as was noted previously (Sun, 2011).

5 Conclusions

In this paper, we fitted the satellite observation SLA data with Gaussian functions. Two intrinsic length scales implied that most eddies are self-similar but that their vertical and horizontal scales are independent. The results indicated that the SLA of the typical ocean eddies are primarily of Gaussian shape (~50%). A greater amplitude was associated with ocean eddies with a more similar shape. In addition, approximately 40% of the ocean eddies are a combination of two Gaussian eddies with different parameters. According to the fitting result, the amplitude shift is relatively large (~10 cm), i.e., larger than the observation data error (~ 3 cm). As a result, the use of shift parameters is required in fitting the eddy shape, at least for the amplitude. In conclusion, the Gaussian shape is a good approximation for the typical shape of the ocean eddies. In theoretical and numerical studies we could use this analytical function as an improved model of ocean eddies.

Acknowledgements We thank the three anonymous reviewers for their constructive suggestions. This work was supported by the National Basic Research Program of China (Nos. 2012CB417402 and 2013CB430303) and the National Natural Science Foundation of China (Grant Nos. 41376017 and 41205126) and the Open Research Fund of Key Laboratory of Atmospheric Composition and Optical Radiation of Chinese Academy of Sciences (Grant No. JJ1102). We thank AVISO for providing the SLA data and the open fund of State Key Laboratory of Satellite Ocean Environment Dynamics (No. SOED1501).

References

Chaigneau A, Gizolme A, Grados C (2008). Mesoscale eddies off Peru in altimeter records: identification algorithms and eddy spatio-temporal patterns. Prog Oceanogr, 79(2–4): 106–119

Chaigneau A, Le Texier M, Eldin G, Grados C, Pizarro O (2011). Vertical structure of mesoscale eddies in the eastern South Pacific Ocean: a composite analysis from altimetry and Argo profiling floats. Journal of Geophysical Research: Oceans, 116(C11): C11025

Chelton D B, Gaube P, Schlax M G, Early J J, Samelson R M (2011b). The influence of nonlinear mesoscale eddies on near surface oceanic Chlorophyll. Science, 334(6054): 328–332

Chelton D B, Schlax M G, Samelson R M (2011a). Global observations of nonlinear mesoscale eddies. Prog Oceanogr, 91(2): 167–216

Chelton D B, Schlax M G, Samelson R M, de Szoeke R A (2007). Global observations of large oceanic eddies. Geophys Res Lett, 34(15): L15606

Dong C, Lin X, Liu Y, Nencioli F, Chao Y, Guan Y, Chen D, Dickey T, McWilliams J C (2012). Three-dimensional oceanic eddy analysis in the Southern California Bight from a numerical product. J Geophys Res, 117: C00H14

Dong C, McWilliams J C, Liu Y, Chen D (2014). Global heat and salt transports by eddy movement. Nature Communications, 5: 3294

Ducet N, Le Traon P Y, Reverdin G (2000), Global high resolution mapping of ocean circulation from TOPEX/Poseidon and ERS-1 and -2, J. Geophys. Res., 105, 19,477–19,478

Early J J, Samelson R M, Chelton D B (2011). The evolution and propagation of quasigeostrophic ocean eddies. J Phys Oceanogr, 41 (8): 1535–1555

Hu J, Gan J, Sun Z, Zhu J, Dai M (2011). Observed three-dimensional structure of a cold eddy in the southwestern South China Sea. J Phys Oceanogr, 116: C05016

Isern-Fontanet J, Garcia-Ladona E, Font J (2003). Identification of marine eddies from altimetric maps. J Atmos Ocean Technol, 20(5): 772–778

Li Q Y, Sun L, Liu S S, Xian T, Yan Y F (2014). A new mononuclear eddy identification method with simple splitting strategies. Remote Sensing Letters, 5 (1): 65–72

Ponte R M, Wunsch C, Stammer D (2007). Spatial mapping of time-variable errors in Jason-1 and TOPEX/Poseidon sea surface height measurements. J Atmos Ocean Technol, 24(6): 1078–1085

Roemmich D, Gilson J (2001). Eddy transport of heat and thermocline waters in the North Pacific: a key to interannual/decadal climate variability? J Phys Oceanogr, 31(3): 675–687

Sun L (2011). A typhoon-like vortex solution of incompressible 3D inviscid flow. Theor Appl Mech Lett, 1(4): 042003

Wu J Z, Ma H Y, Zhou M D (2006). Vorticity and Vortex Dynamics. Berlin-Heidelberg: Springer-Verlag. XIV, 776 p., 291 illus

Yang G, Wang F, Li Y, Lin P (2013). Mesoscale eddies in the northwestern subtropical Pacific Ocean: Statistical characteristics and three-dimensional structures. Journal of Geophysical Research: Oceans, 118(4): 1906–1923

Zhang Z G, Zhang Y, Wang W, Huang R X (2013). Universal structure of mesoscale eddies in the ocean. Geophys Res Lett, 40(14): 3677–3681